Influence of CNTs, ZnO, Gd2O3 and SiO2 on Calcium Silicate Hydrate: A Raman spectroscopic study

Muhammad Azeem (mazeem@sharjah.ac.ae)
University of Sharjah

Research Article

Keywords: CNTs, ZnO, Gd2O3, SiO2, CSH, ordinary Portland cement (OPC)

Posted Date: September 17th, 2021

DOI: https://doi.org/10.21203/rs.3.rs-895716/v1

Abstract

Raman spectra are collated from the cement paste matrices of CNTs, ZnO, Gd_2O_3, and SiO_2. The spectra show that CNTs do not take part in hydration process and therefore concentration of calcium silicate hydrate (CSH) is unchanged in CNT-OPC matrix. The metal oxides, on the other hand, have shown significant effects on the CSH concentration. The CSH concentration increases with the increase of ZnO weight percent in the matrix whereas spectra collected from Gd_2O_3 matrix shows the strongest CSH vibrational bands. Moreover, vibrational bands of $CaCO_3$ also become weak in the matrices with Gd_2O_3. The addition of SiO_2 however had opposite effects that is by increasing the weight percent of SiO_2 in the matrix, the CSH concentration is decreased. Since CSH acts a glue in a binder, the study shows that its concentration can be controlled by adding foreign elements. Such binders are expected to show improved strength and durability.

Introduction:

The quest to reduce the environmental impact of the cement and the concrete industry has led the researchers to the path of developing composite construction materials. However, the research on these materials is limited to academic settings and no large scale industrial applications are realized yet. This is partly due to poor understanding of the formation of reaction products and hydration kinetics in the composite construction materials. Although, it is well understood that the main reaction product after the hydration of the Portland cement is calcium silicate hydrate (CSH) and calcium hydroxide(CH), it is not known that how these will be effected if the foreign elements are added to the cement.

Choice of dopants is extraordinarily wide to make cement paste matrix. There are studies reporting mixing of ordinary Portland cement (OPC) with a combination of micro- and nanomaterials and their effect on the mechanical[1,2], physical[3,4], microstructural and durability properties of concrete[5–7]. Generally, it is considered that the foreign impurities fill the voids making a dense and inhomogeneous matrix. However, overall electronic and crystal structures of the matrix also changes if the impurities consist transition metals[8]. An enhanced hydration activity and deformed crystal structure is observed with barium doped dicalcium silicate[9]. The addition of nano-limestone changes the calcium to silicon ratio[10,11], which naturally alters the crystal structure and the physical properties of the matrix. The carbon based nanostructures[12–15] exhibit an improved elastic modulus and flexural toughness. When reinforced with hybrid CNT-graphene micro nanoparticles(GMNP)[16,17], the matrix as also helps to resist bio-corrosion [18]. Interestingly, the mechanical strength [12] and the flowability [19] is found to decrease with the increase of the CNTs in the cement paste matrix. Other factors affecting the physical and mechanical[20] properties of such concretes are the density and the types of pure or impure silicates[6], sulphates and aluminates[21] compounds [6,11,22], water to cement ratio[10,23,24], and calcium to silicon ratio[25–27].

On the other hand, dopants may also have a profound quantitative effect on the hydration products. In this study, we have used Raman spectroscopy to gain insight of formation of the calcium silicate hydrate

in presence of the metal oxides. The cement paste matrix is prepared with ZnO, Gd_2O_3 and SiO_2 and three types of carbon nanotubes (CNTs); pristine, hydroxyl (OH) and carboxyl (COOH) functionalized. All three oxides are insulators and have propensity to react with the components of OPC and water. Carbon nanotubes on the other hand do not chemically react, however, there is an electrostatic interaction present between the CNTs and the composites of the OPC[12]. The Raman spectra shows a clear evidence that the oxides take part in the hydration process and have direct effects on the CSH formation. Further, it is also observed that the presence of the oxides also has effect on the concentration of the calcium carbonate.

Materials And Methods:

The process of the sample fabrication is described in detail in the references[28]. Brifely, the ordinary Portland cement (OPC) of Type I was used for the preparation of cement paste matrices with water to cement ratio of 0.4 for all the samples. The carbon nanotubes (CNTs) were obtained from Sisco Research Laboratories (SRL) and the zinc oxide (ZnO) and the silicon oxide (SiO_2) were purchased from the Sigma-Aldrich whereas gadolinium oxides (G_2O_3) were obtained from American Elements. All oxides were in a 99.9% purity state. The CNTs were of three types: pristine, hydroxyl functionalized (–OH) and carboxyl (–COOH) functionalized. The average lengths of all three types of the CNTs were around 10–30 μm and the diameters were on average approximately 30–50 nm. Dopants were mixed in water first, by using a bench mixer. To ensure the near uniform mixing, the mixing was carried out for two minutes. With the mixer running, the OPC powder was gradually added to the mixture and the mixing was carried out 15 minutes. Afterwards, the matrices was poured in to the steel moulds of size 50 mm cube and a table type external vibrator was used for the compaction. Specimens were demolded after 1 day and then dipped in the water for four weeks.

The experimental Raman spectra was obtained by using Renishaw inVia confocal Raman microscope. A set of 10 spectra were collected from various locations of each sample to obtain the average. In each recording, a site of a specimen was exposed for 10 seconds to a 785 nm wavelength laser with a spot size of 50 μm and a laser power of 1% (14 mW). The spectral range was kept between 100 cm-1 and 1400 cm-1, which represent the fingerprint region for finding signature peaks from the hydration products. For the CNT-cement paste matrices, the spectral range was from 200 cm^{-1} to 3000 cm^{-1}. The spectra were collected at the wavelength intervals of 500 cm^{-1} and then combined to obtain the full spectrum.

Experimental Raman Spectra:

Ordinary Portland cement and the cement paste:

The Raman spectrum for the OPC powder and the corresponding values for each of the Raman vibrational bands are shown in the Fig. 1.

The Raman bands at 373 cm^{-1}, 419 cm^{-1}, 458 cm^{-1}, 578 cm^{-1}, 604 cm^{-1}, 843 cm^{-1} and 1009 cm^{-1} are contributed by the alite molecules whereas the belite contribution can be identified by the signals at 659 cm^{-1} and 927 cm^{-1}. A peak at 258 cm^{-1} seems to be the net effect of the alite and the belite molecules. A carbonate ($CaCO_3$) peak is at 1087 cm^{-1} is well known and the vibrational bands at 1165 $cm^{-1}$and 1245 cm^{-1} are identified as the calcium sulphate ($CaSO_4$) and potassium sulphate (K_2SO_4), respectively.

The spectrum obtained from a control sample of the cement paste is shown in the Fig. 2. The vibrational modes at 292 cm^{-1} and 368 cm^{-1} are present, mainly, due to the bond stretching between the silicon and the oxygen atoms of the alite hydrate and the $CaH_2O_5Si^{-2}$. The calcium sulphate dihydrate are at 466 cm^{-1}, 844 cm^{-1}, 1164 cm^{-1} and 1355 cm^{-1}. The calcium aluminum hydride (Al2CaH8) phase is identified at about 713 cm^{-1}. An experimental CSH band at the 1255 cm^{-1} is due to CaH_2O_4Si whereas all other CSH bands are contributed by $CaH_2O_5Si^{-2}$[13].Most of the cement paste is, therefore, made up of calcium silicate hydrate (CSH) with a chemical formula $CaH_2O_5Si^{-2}$. As opposed to other CSH configurations, such as CaH_2O_4Si and $Ca_2H_2O_5Si$ where the formal charge is 0, this molecular composition has a formal charge of − 2 indicative of a reactive substance.

CNT-cement paste matrix

The Raman spectra from the cement paste mixture with 0.2 wt% and 0.4 wt% of the pristine CNTs (P-2% and P-4%), CNTs-OH (OH-2% and OH-4%) and the CNTs-COOH (COOH-2% and COOH-4%) are shown in the Fig. 3 in the frequency range 200 cm^{-1} to 3000 cm^{-1}. The hydrated products are identified in the first half of the frequency range, from 200 cm^{-1} to 1400 cm^{-1}. The features of the spectra are indistinguishable for different concentrations of CNTs and with that of the cement paste, (Fig. 1) showing that the CNTs do not participate in the hydration reaction. The apparent splitting of the G band at 1587 cm^{-1} and 1624 cm^{-1} occurs due to the shear force applied during mixing of the cement paste[29] as some of the CNTs are graphitized. The hydrated crystals grown at the CNT sites apply tensile stress on the CNT surface causing the D and the D overtone bands to shift to the lower frequencies, at 1319 cm^{-1} and 2637 cm^{-1}, respectively. The growth of the $CaH_2O_5Si^{-2}$ as a major phase and the structural defects in the CNTs, which results in the charge imbalance at the surface of CNT, enhances the electrostatic interaction and thus strengthens the concrete. The D and D overtone bands are more intense in the specimens which higher concentrations of CNTs (P-4%, OH-4% and COOH-4%). A high I_D/I_G ratio (> 1) in these specimens indicates greater degree of the structural defects in the CNTs affecting the strength of the concrete[12].

ZnO, Gd_2O_3 and SiO_2matrices with cement

The cement paste mixtures with oxides show some remarkable differences compared to the control samples as shown in the Fig. 4. Strong CSH peaks are visible at 154 cm^{-1} for ZnO and Gd_2O_3 which is a common feature with the control samples. This peak, however, is very weak in the cement paste matrix with SiO_2. Another interesting feature would be a weak peak at 207 cm^{-1} in ZnO-cement paste with its

counterpart at 211 cm^{-1} in Gd_2O_3 cement paste. This feature is absent in in the control and SiO_2 cement mixtures. A strong CSH vibrational mode is visible at 281 cm^{-1} in the control and ZnO-cement paste but weaker in Gd_2O_3 and SiO_2 at about the same position. The CSH vibrational band at 357 cm^{-1} in the control samples, and ZnO and SiO_2 matrices with the cement however it is considerably strong in the Gd_2O_3-cement paste matrix. The vibrational band contributed by the calcium sulphatedihydrate (CaH_4O_6S) is rather weak in the control samples at 464 cm^{-1} which is also shared with the ZnO and Gd_2O_3 matrices but, interestingly, is completely absent in the SiO_2 cement paste. Next, a broad and strong CSH band at 605 cm^{-1} in the control sample is shared by all the matrices. However, it is significantly stronger in the SiO_2 and Gd_2O_3 matrices. The contribution from the calcium aluminum hydride (Al_2CaH_8) is at around 711 cm^{-1} in the control and ZnO cement paste but is absent in the SiO_2 and Gd_2O_3 matrices. Further, a doublet in the control, at 844 cm^{-1} and 856 cm^{-1}, supposedly contributions from the $C\bar{\bar{S}}H_2$ and CSH respectively, is replaced by a single but broad band at around 846 cm^{-1}. A weak CSH band at approximately 926 cm^{-1} is also a common feature with the all the mixtures. Another calcium sulphatedihydrate band at about 986 cm^{-1} is weak in control and ZnO matrix but reasonably strong in the SiO_2 and Gd_2O_3 matrices. A very strong calcium carbonate band in control and ZnO has become relatively less strong in the SiO_2 and Gd_2O_3 matrices. A weak $C\bar{\bar{S}}H_2$ band in control at 1168cm^{-1} has become slightly more prominent. Finally, a vary clear CSH band at 1254 cm^{-1} has become poorer in rest of the samples.

A similar trend is observed in the specimens with 0.4wt% of the same impurities with very little differences. The spectrum of 0.4wt% SiO_2-cement matrix now show strong and narrow peaks at approximately 154 cm^{-1}, 282 cm^{-1} and a very strong calcium carbonate peak at around1080 cm^{-1}. These features are missing in the specimens prepared with 0.2wt% of SiO_2. Another major difference is that the CSH band in the specimens with 0.4wt% of SiO_2 now show relatively weaker band at 605 cm^{-1} whereas in the 0.2wt% specimens, this is the strongest band. On the other hand, the CSH band at 605 cm^{-1} has become stronger in the 0.4wt% ZnO-cement paste samples compared to 0.2wt%. The same band is unchanged in its intensity in Gd_2O_3-cement mixture in both the samples prepared with 0.2wt% and 0.4wt% with the difference that the later shows bands with narrower peak width. It should be noted that the CSH band at 605 cm^{-1} is the stronger in all the samples with oxide impurities when compared with control and CNT-cement paste matrices. It is a clear manifestation of the fact that the oxide impurities have somehow a dramatic effect in increasing the hydration process.

Discussion:

For the case of oxide impurities, a clear pattern seems to emerge in the Raman spectra. The vibrational band at 207 cm^{-1} is the contribution of zinc hydroxide (ZnH_2O_2). Since, tricalcium silicate (C3S) is a major mineral in the OPC, its chemical reaction with ZnO can be written as,

$3CaO.SiO_2 + 3H_2O + ZnO \rightarrow 2CaO.SiO_2.H_2O + CaH_2O_2 + ZnH_2O_2$.

A similar reaction is expected to take place with the dicalcium silicate (C2S), as well.

The chemical reaction of Gd_2O_3 with the C3S is,

$3CaO.SiO_2 + 5H_2O + Gd_2O_3 \rightarrow 2CaO.SiO_2.H_2O + CaH_2O_2 + 2GdH_3O_3$

The signature peak from GdH_3O_3 is seen at 211 cm^{-1} in the Raman spectrum. Although, the hydration process of tricalcium silicate is complex and not completely understood. A general chemical equation is,

$3CaO.SiO_2 + 2H_2O \rightarrow 2CaO.SiO_2.H_2O + CaH_2O_2$.

From the chemical equations, it can be immediately realized that the number of water molecules participating in the reaction is increased when metal oxides are added to the cement paste. The hydration process, therefore, is more effective in the presence of ZnO and Gd_2O_3 indicated by the increase of the CSH concentration in the matrix shown in the Raman spectra.

For the case of ZnO, we observe that the CSH Raman band at 605 cm^{-1} is stronger for the ZnO 0.4 wt% cement paste. Whereas, the same band in the Gd_2O_3 matrix is far more stronger compared to ZnO and is equally strong for both, 0.2wt% and 0.4wt% specimens. Moreover, the spectra of Gd_2O_3 matrices also show that the calcium carbonate peaks have become weak at around 1080 cm^{-1} which is not the case with matrices prepared with ZnO. It should be noted that C3S and C2S are never in their purest form in OPC. Rather, the chemical formula turns out to be Ca3.09Si0.63Fe0.22A0.14Mg0.06S0.05Ti0.01K0.01Cr0.01 and Ca2.48Si0.51Fe0.18Al0.11Mg0.05S0.04Ti0.01K0.01 for C3S and C2S respectively[13]. Therefore, Ca/Si ratio is greater than 5 indicating that the tobermorite and jennite are far from being perfect crystals and there are Si vacancies. These vacancies are occupied by the Zn and Gd atoms thus modifying the crystal structure significantly. The Gd^{3+} is a rare earth metal and has propensity to oxidize[30,31] very quickly therefore there are not enough oxygen atoms to form carbonates in the Gd_2O_3 matrix with OPC. On the other hand, SiO_2 matrix shows an interesting behavior. While, the CSH products are high for the 0.2 wt% of SiO_2, it decreases quite significantly when its concentration is increased to 0.4wt%. This is in agreement with a previous study[32] which shows that the increasing SiO_2 concentration in the OPC paste, the space between the CSH domains also increases thus creating pores and voids which reduces the compressive strength of the specimen.

Conclusion:

The concentration of the CSH in the cement matrix with CNTs, ZnO, Gd_2O_3 and SiO_2 is measured by Raman spectroscopy. It is observed that the CNTs do no participate in the hydration process and therefore, CSH concentration is unchanged in the resultant matrices when compared to the control.

However, metal oxides actively participate in the hydration process and form new hydrates as well as have a definitive effect on the CSH concentration in the matrix. The Raman spectrum of the ZnO-OPC matrix show a strong CSH vibrational band indicating that the concentration of CSH increases with the increase of the ZnO weight percentage in the matrix. Similarly, a strong CSH band is observed in Gd_2O_3 cement matrix as well. However, more interestingly, the $CaCO_3$ band has become significantly weak in Gd_2O_3 cement matrix. This indicates that the Gd^{3+}, with their strong ability to form oxides and hydrides, have bonded with the CO_2 in the atmosphere. Finally, for SiO_2, CSH concentration weakens when weight% of the SiO_2 is increased. This is in line with the previous studies where decreasing Ca/Si also caused the compressive strength to fall. While, compressive strength data is available for OPC matrices with CNTs and SiO_2, it is not clear what will be mechanical behavior of the ZnO and Gd_2O_3 matrices with OPC. However, based on the observations presented in this study, it can hypothesized that an improved compressive strength can expected from these specimens as the concentration of the hydration products, including CSH is much improved.

References

1 K. Gong, S. M. Asce, Z. Pan, A. H. Korayem, D. Ph, L. Qiu, D. Li, F. Collins, C. M. Wang, W. H. Duan and A. M. Asce, 2015, **27**, 1–6.

2 F. U. A. Shaikh, S. W. M. Supit and S. Barbhuiya, 2017, **29**, 1–10.

3 J. Han, Y. Liang, W. Sun, W. Liu and S. Wang, 2015, **27**, 1–14.

4 M. A. Kafi, A. Sadeghi-nik, A. Bahari, A. Sadeghi-nik and E. Mirshafiei, 2016, **28**, 1–10.

5 F. U. A. Shaikh and S. W. M. Supit, 2016, **28**, 1–7.

6 W. Han, T. Sun, X. Li, M. Sun and Y. Lu, *Nucl. Instruments Methods Phys. Res. Sect. B Beam Interact. with Mater. Atoms*, 2016, **381**, 11–15.

7 Z. Lu, C. Lu, C. K. Y. Leung and Z. Li, *Cem. Concr. Compos.*, 2019, **98**, 83–94.

8 Y. Tao, W. Zhang, D. Shang, Z. Xia, N. Li, W. Y. Ching, F. Wang and S. Hu, *Cem. Concr. Res.*, 2018, **109**, 19–29.

9 L. Chi, A. Zhang, Z. Qiu, L. Zhang, Z. Wang, S. Lu and D. Zhao, *Nanotechnol. Rev.*, 2020, **9**, 1027–1033.

10 B. Lothenbach, G. Le Saout, E. Gallucci and K. Scrivener, *Cem. Concr. Res.*, 2008, **38**, 848–860.

11 W. Li, W. H. Duan, X. Li, S. J. Chen, G. Long and Y. M. Liu, *J. Mater. Civ. Eng.*, 2017, **29**, 04017087.

12 M. Azeem and M. Azhar Saleem, *Constr. Build. Mater.*, 2020, **239**, 117875.

13 M. Azeem and M. Azhar, *Constr. Build. Mater.*, 2020, **264**, 120691.

14 N. M. Hassan, K. P. Fattah and A. K. Tamimi, *Constr. Build. Mater.*, 2017, **154**, 763–770.

15 A. Tamimi, N. M. Hassan, K. Fattah and A. Talachi, *Constr. Build. Mater.*, 2016, **114**, 934–945.

16 A. Akbar, K. M. Liew, F. Farooq and R. A. Khushnood, *Constr. Build. Mater.*, 2020, 120721.

17 M. Jung, Y. soon Lee, S. G. Hong and J. Moon, *Cem. Concr. Res.*, , DOI:10.1016/j.cemconres.2020.106017.

18 V. Stroganov, E. Sagadeev, R. Ibragimov and L. Potapova, *Constr. Build. Mater.*, 2020, **246**, 118506.

19 S. K. Adhikary, Ž. Rudžionis and R. Rajapriya, *Sustain.*, 2020, **12**, 1–25.

20 T. Liu, Y. Wang, K. Zhou, F. Gao and S. Xie, *Adv. Civ. Eng.*, , DOI:10.1155/2019/6805480.

21 L. Black, C. Breen, J. Yarwood, C. S. Deng, J. Phipps and G. Maitland, *J. Mater. Chem.*, 2006, **16**, 1263–1272.

22 M. Szeląg, *Constr. Build. Mater.*, 2018, **189**, 1155–1172.

23 F. Liu and Z. Sun, *Front. Struct. Civ. Eng.*, 2016, **10**, 168–173.

24 H. F. W. Taylor, *Cement Chemistry*, Thomas Telford, London, 2nd edn., 1997.

25 S. Grangeon, F. Claret, C. Roosz, T. Sato, S. Gaboreau and Y. Linard, *J. Appl. Crystallogr.*, 2016, **49**, 771–783.

26 S. A. Miller, S. A. Pacca and A. Horvath, *Cem. Concr. Res.*, 2018, **114**, 115–124.

27 S. S. Kutanaei, D. Ph and A. J. Choobbasti, 2017, **29**, 1–9.

28 M. Azeem, M. T. Junaid and M. Azhar, *Constr. Build. Mater.*, 2021, **305**, 124748.

29 X. Zhao, Y. Ando, L.-C. Qin, H. Kataura, Y. Maniwa and R. Saito, *Appl. Phys. Lett.*, 2002, **81**, 2550–2552.

30 M. Azeem, *Chinese Phys. Lett.*, , DOI:10.1088/0256-307X/33/2/027501.

31 M. Azeem, in *MRS Advances*, 2017, vol. 2.

32 W. Kunther, S. Ferreiro and J. Skibsted, *J. Mater. Chem. A*, 2017, **5**, 17401–17412.

Figures

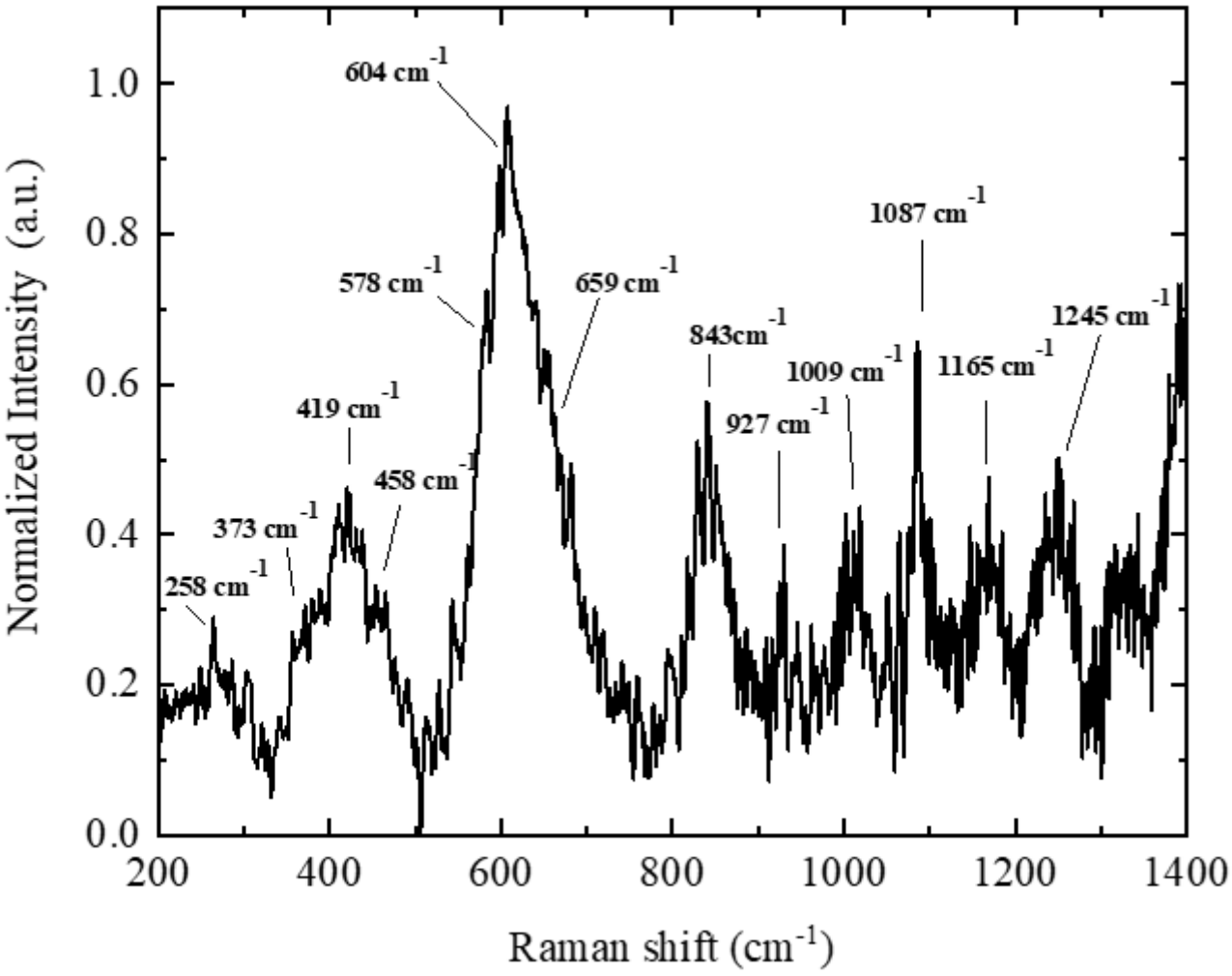

Figure 1

Experimental Raman spectrum for OPC powder

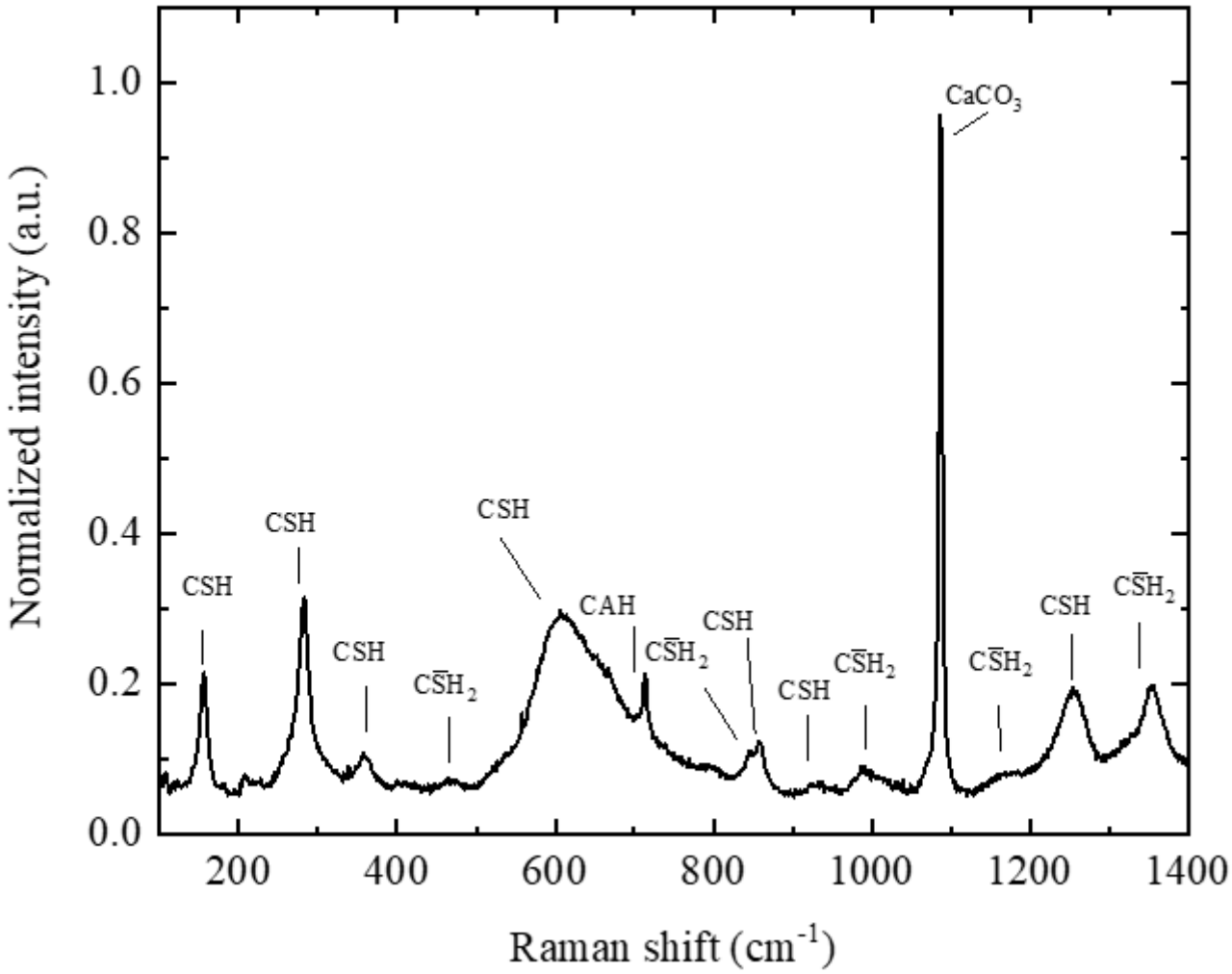

Figure 2

Experimentally obtained spectrum from a control sample of cement paste

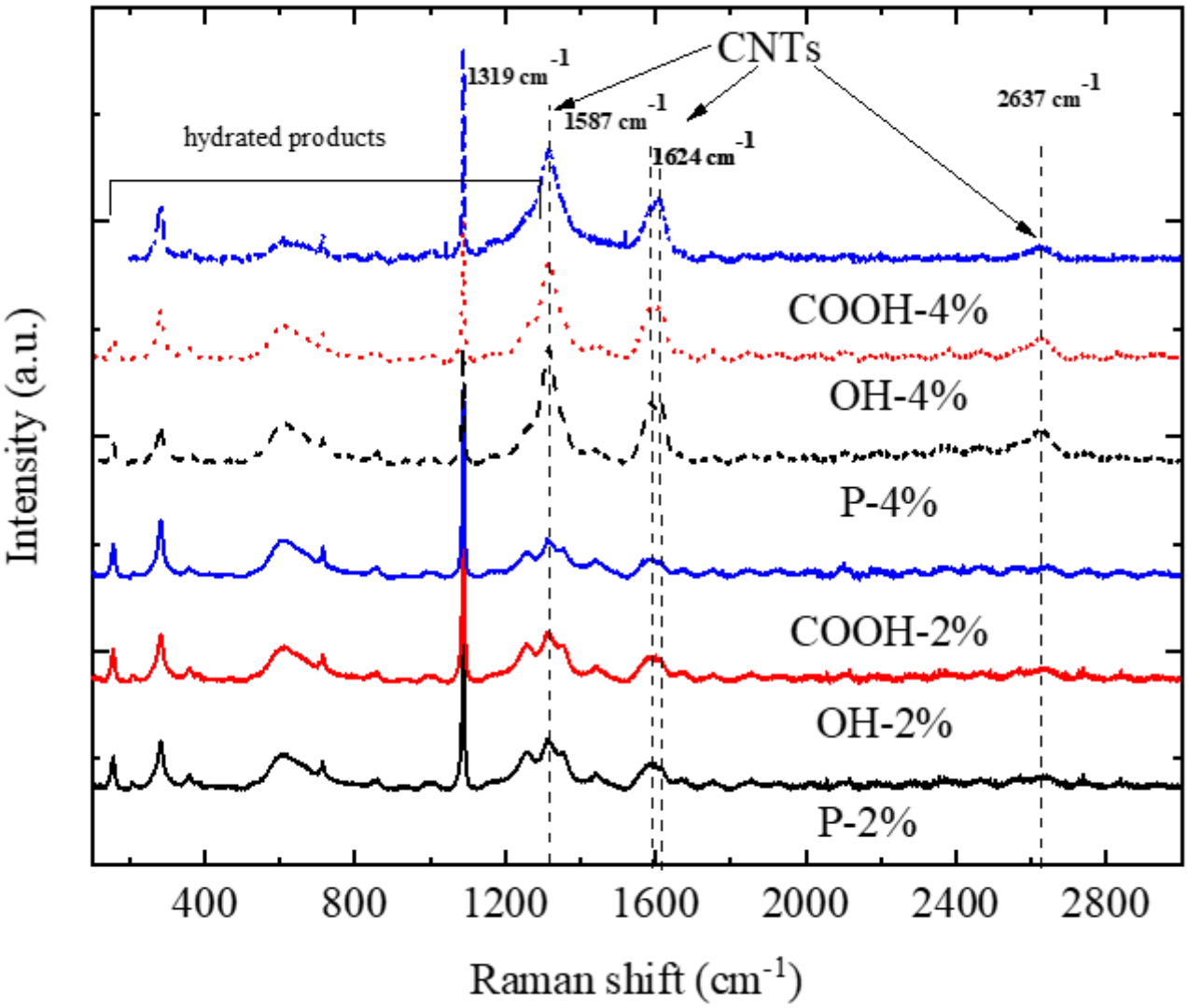

Figure 3

Raman spectra from the CNT-cement paste matrix

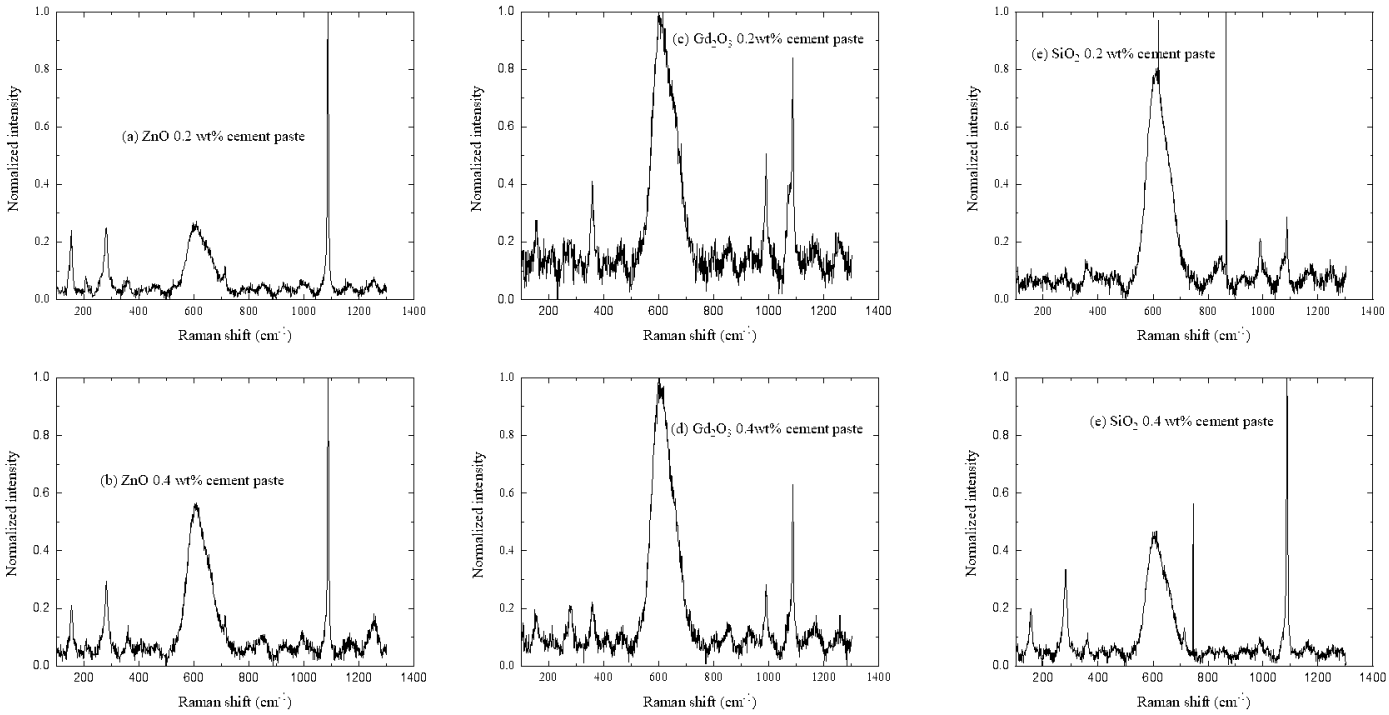

Figure 4

Raman spectra for cement paste matrices of oxides.